6th International Conference on Advances in Experimental Structural Engineering
11th International Workshop on Advanced Smart Materials and Smart Structures Technology
August 1-2, 2015, University of Illinois, Urbana-Champaign, United States

Seismic Behavior of Composite Beams under Damper and Frame Forces of Shifted Phases : Finding from Full-Scale Tests of Buildings and Subassemblies

Kazuhiko KASAI[1], Yoriyuki MATSUDA[2]

1 *Professor, Structural Engineering Research Center, Tokyo Institute of Technology, Suzukakedai, Japan. E-mail: kasai@serc.titech.ac.jp*
2 *Graduate Student, Dept. of Built Environment, Tokyo Institute of Technology, Suzukakedai, Japan. E-mail: matsuda.y.ag@m.titech.ac.jp*

ABSTRACT

Supplemental-damping technology is suitable for a steel frame because of ease for connecting dampers and relatively low frame stiffness requiring drift control. During an earthquake, the members surrounding the damper are subjected to combined bending moment and axial force produced cyclically by the actions of the damper and frame, respectively. Damper force and damper deformation have shifted phase, and the latter is in-phase with the frame story drift, which makes phase difference between the moment and axial force.

These as well as slab and beam composite actions, and stress concentrations at the gusset plate for connecting damper make beam behavior complex, and they are discussed by analyzing data from the two experimental projects; shake-table tests of a full-scale 5-story building, and cyclic tests of the beam-column-gusset plate subassemblies. The cyclic test employs a newly developed loading method alternating displacement control for story drift, and force control for damper force whose target value is calculated step-by-step by a hybrid scheme using the numerical model of the damper.

When analyzing the data, two contributions having phases of story drift and damper force, respectively, are extracted from each of the forces shared by the steel beam, concrete slab, gusset plate, and their corresponding strains. The results as well as implication to analysis/design of the members and connections in the damper bay are discussed.

KEYWORDS: *Passive control, Dampers, Composite beam, Full-scale test, Subassembly test, Gusset plate*

1. INTRODUCTION

1.1 General

Recent earthquakes in Japan have led to greatly increased use of supplementally-damped systems in order to protect the buildings and to assure continuity of their functions. Steel frames are suited to the technology because of ease for connecting dampers and relatively low frame stiffness requiring drift control. As depicted in Figure 1a for the undamped frame, the beam not connected to dampers primarily develops bending moment synchronized with the story drift during an earthquake. Whereas in Figure 1b for the damped frame, the beam in a supplementally-damped system connected to typical brace-type damper develops combined bending moment and axial force. At early stage of increasing story drift, the damper force and consequently the beam axial force quickly increases, while the beam moment increases rather slowly in proportion to the story drift. Therefore, beam axial force and moment have different phase and time lag, which is the key point in this paper.

From now on, we define the “frame action” as development of beam and column bending moments due to the story drift, and “damper action” as development of damper axial force and consequently the beam and column axial forces. Summarizing above discussions, undamped frame response is caused by frame action only, whereas the damped frame response is caused by both frame and damper actions. It also should be noted that the phase of the damper force depends on the hysteretic characteristics as shown in Figure 2 for major dampers in Japan. Although the dampers are accurately modelled and their properties are well understood, it is not the case

for the frames. Common problem in design of both undamped and damped frames is inadequate knowledge on composite beam stiffness and strength against the frame and damper actions as discussed below:

Recent shake-table tests of full-scale buildings by the writers[1-5] (e.g., Figure 3a) and others[6-8] indicated that the composite beam under frame action accompanied by negative beam bending was substantially stiffer than the bare steel beam, in contrary to the non-composite action considered in design specifications. The stiffness was not as high as positive bending case, but was certainly high enough to consider in analysis and design. It is also not known whether or not such behavior can change with the presence of axial force caused by the damper action. In a "positive loading case" depicted by Figure 1b, the beam in the damped frame is subjected to positive bending moment causing compression in slab, and at the same time tension in the beam and slab. Whereas in "negative loading case", the situation will be reversed. Further, whether slab will be in tension or compression depends on relative magnitudes of the two actions as well as their nonlinearities (Figure 1b).

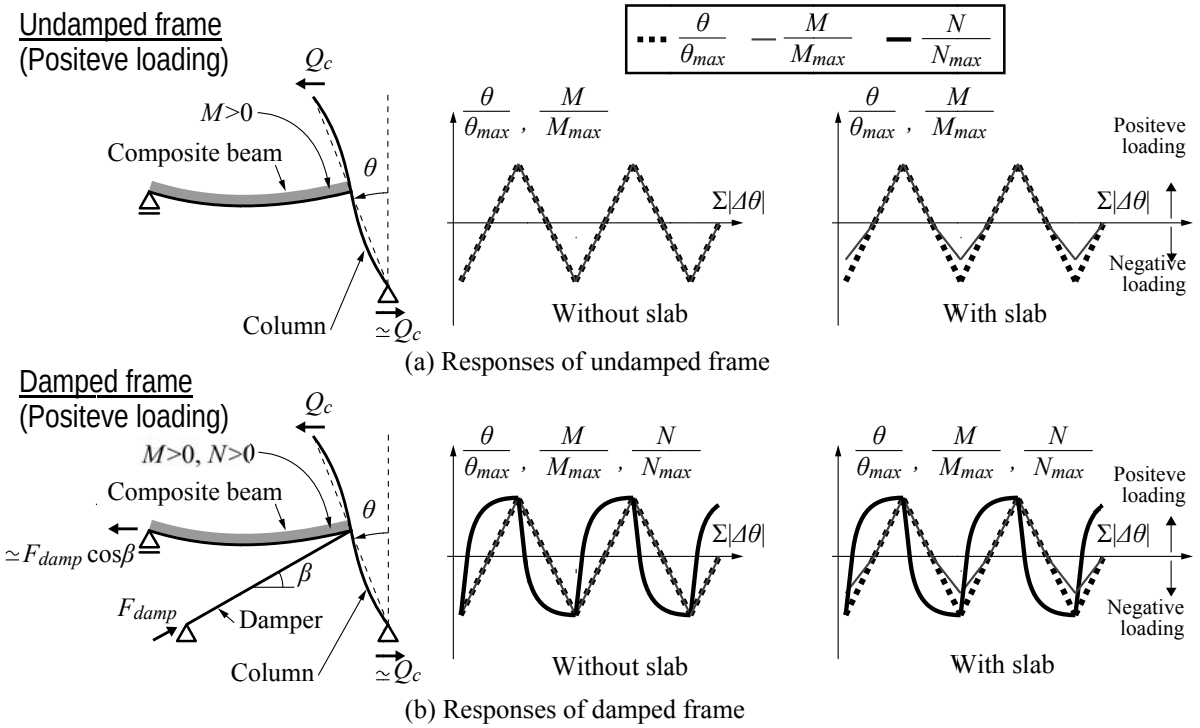

Figure 1 Deformed shape of (a) undamped and (b) damped frames under positive loading, and histories of drift angle θ, beam moment M, and axial force N

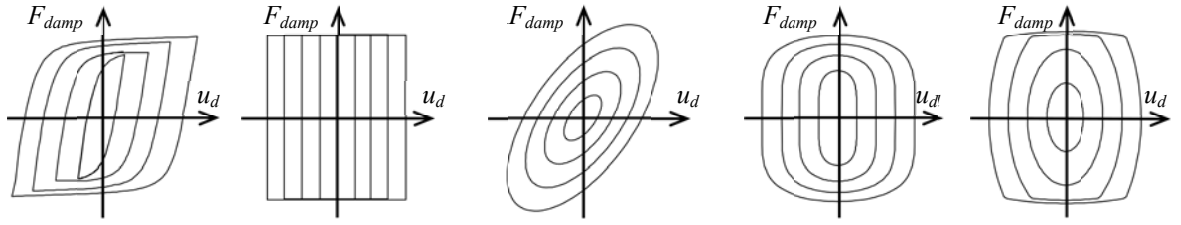

Figure 2 Force – deformation relationship of steel, friction,viscoelastic, viscous, and oil dampers (damper axial responses)

1.2 Objectives and Scopes

The protective system should be a predictable structure for its seismic performance, enabling reliable estimate for future structural/nonstructural damage and functional continuity of the building. In the supplementally-damped system, composite beam that significantly influences the frame property has not been fully understood for its stiffness, elastic limit, and interaction with connection such as a gusset plate. The concrete slab drastically changes responses of the steel beam and connections, and the past research is insufficient to clarify the issue. Hence, studies revisiting issues of stiffness, strain, and stress in the composite

beam as well as new studies on axial and bending load on the composite beam, and gusset plate connection behavior are being conducted at Tokyo Institute of Technology. The objectives of this paper are to discuss the above issues on various composite behaviors and to clarify their relations with frame and damper actions. The behaviors observed from two types of full-scale tests are considered. Special experimental methods for data analysis as well as loading control are proposed. The paper is written according to each test as follows:

The first part is based on shake-table tests of a full-scale 5-story steel frame building (Figure 3a). The tests were conducted by inserting and replacing 4 different types of dampers or by completely removing them. The world's largest shake table E-defense was used, and the frame remained almost elastic even under the shaking using the one of the catastrophic ground motion recorded during the 1995 Kobe earthquake. The frame was instrumented with abou 1,400 sensors, and the proposed data analysis method will be used to obtain internal moments, shear forces, and axial forces of all beams and columns. damped frame, they are obtained based on the phase difference of the frame and damper actions. The composite beam stiffness is compared with bare beam stiffness, and effective slab width is estimated for positive and negative bending in both undamped and damped frames.

The second part is based on full-scale subassembly tests by simulating the frame and damper actions, respectively (Figure 3b). Story drift is controlled to simulate the frame action, and the damper force is controlled to simulate the damper action. The target damper force is calculated at each step based on the current state of frame and corresponding damper deformations. It is a simplified hybrid test combining the displacement and force controls. Obtained strain distributions are decomposed into frame and damper action components, respectively. The specimens with and without the slab are compared. A method combining the two actions differently to predict strain distributions for hypothetically selected force magnitude and/or damper hysteretic type is proposed.


(a)
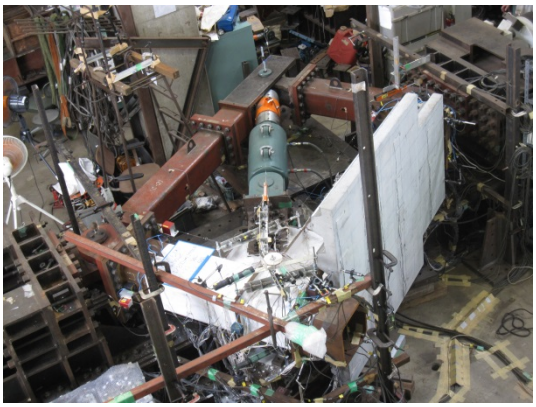
(b)

Figure 3 (a) Exterior view of the building specimen, and (b) subassembly specimen

2. FULL-SCALE 5-STORY STEEL BUILDING WITH STEEL DAMPERS

2.1 Outline of Full-Scale Tests

As shown in Figures 4 and 5, the building is 5-story with two bays in each direction. The plan dimension is 10m×12m, and total height from the upper surface of a stiff foundation beam is 15.8 m. Total seismically active weight of the superstructure is 4,730 kN. The frame consists of steel members, and all nine columns in Figure 5 are 350 x 350 mm box column sections with thickness varying from 12 to 22mm. There are nine "undamped" bays, of either 5 or 7 m span and only three "damped" bays of 5 m span containing dampers. In Y-direction (Figure 5), there are only one damped frame, in contrast to X-direction having two damped frames. The damper therefore is the largest in Y-direction, having twice capacity than the dampers in X-direction. The beam-column connections are of fully-restrained type for both undamped and damped frames.

Each span consists of three beam portions, two end portions are 0.825 and 1.075 m long from column face in the undamped and damped frames, respectively. In center portion, all beams are wide-flange sections with 400 mm depth and 200 mm width, and web thickness varies from 9 to 12 mm and the flange thickness from 12 to 22 mm.

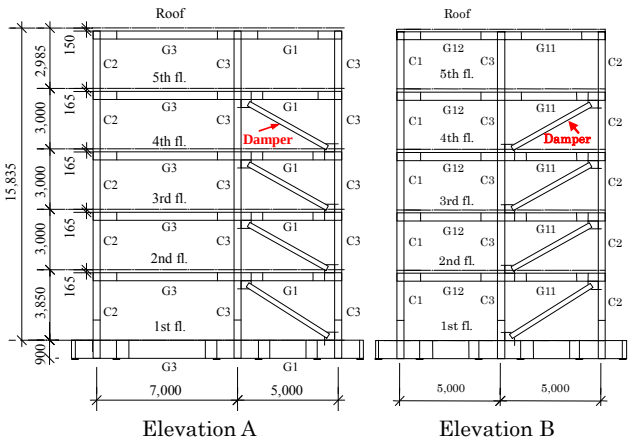

Figure 4 Elevation for full-scale 5-story building

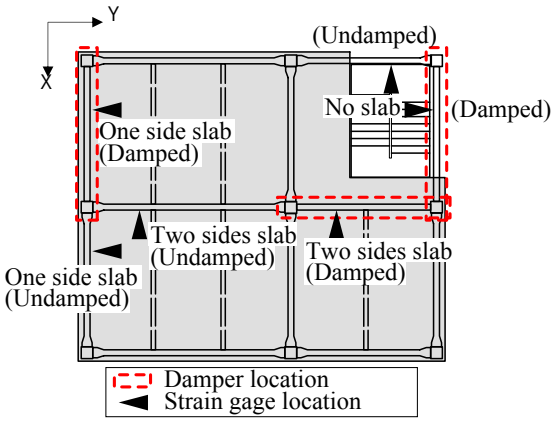

Figure 5 Plan, damper locations, and strain locations

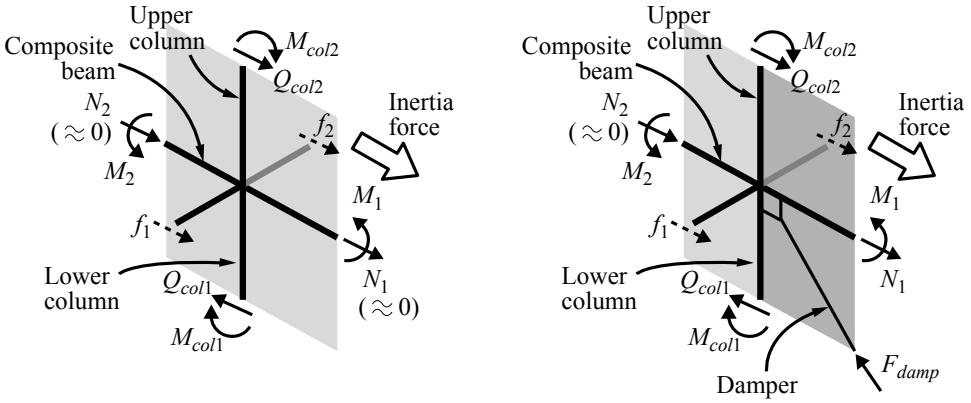

(a) Undamped & Undamped frames (b) Undamped & Damped frames

Figure 6 Horizontal forces and bending moments in the undamped and damped frames

For the undamped frame (Figure 5), the flange and web of the end portions are thicker than those of the center portion, and the flange is haunched to delay yielding. The three portions are bolt-connected together through the splice plates on flanges and webs as will be shown later. As for the damped frames (Figure5), the three portions have a uniform section to resist large axial forces transmitted from the damper, and their flanges are connected by butt-weld to assure continuity. No haunch is used due to already large section created by the gusset plate (Figure 4). The concrete slab with corrugated metal deck is used at typical floors, and the height of the slab is 155mm, with depth of corrugated deck 75mm. The deck runs in Y- direction. The roof slab has uniform thickness of 150mm. Single line of shear studs of 19 mm diameter is used with spacing of 200 mm.

For the economical reason the building was tested repeatedly by varying the damper type. In the order of the test performed, four different types of dampers, steel, oil, viscous, and viscoelastic dampers, are used (Figure 2), but only the test with steel dampers is considered in this paper. Mostly, the 4th floor beams in either undamped frame or damped frame, having no slab, slab on one side, and slab on two sides of the beam (Figure 5) will be discussed. Thus, six (= 2 types of frames x 3 situations of slab) different beams are considered in this study, and they are depicted in Figure 5. In the building test, the three-direction ground motion recorded at the JR Takatori station during the 1995 Kobe earthquake was scaled 0.05, 0.1, 0.2, 0.4, and 1.0 times. However, only unscaled ground motion will be considered here, and will be named as “Takatori ground motion” from now on. The maximum story drift angle between the 3rd and 4th floors was 0.60% rad in both X- and Y-directions, whereas those throughout building height were 0.66% between the 1st and 2nd floors, and 0.81% between the 2nd and 3rd floors, respectively.

2.2 Composite Beam Internal Force Estimations from Steel Strains and Their Phases

This section proposes a method to determine the forces in the composite beams of undamped and damped frames in Figure 6 based on the strains recorded from the steel beam portion only. It determines bending moment M and axial force N of the composite beam (Figure 6b), and internal forces such as the slab axial force N_c, steel beam axial force N_s, and bending moment M_s. The strain gages were attached to two sections at

every span of the building. Typically their distance from the closest column centerline is either 0.21 or 0.26 times 7 m span length, and 0.31 or 0.34 times 5 m span length. These locations are selected to maintain strains elastic and to avoid possible disturbance caused by the gusset plate, beam splice, horizontal haunch, and others.

Figure 6a shows undamped frames with horizontal forces and bending moments, where typically $N = 0$ can be assumed, and an earlier method (Suita et al. 2009, Yamada,2009 and Kasai et al., 2011) shown in Figure 7 will be used. As will be demonstrated, recorded steel strains in the composite beam distributed almost linearly. Thus, assuming plane section for the steel beam portion, average strain $\varepsilon_s^{(i)}$ and curvature $\varphi_s^{(i)}$ at the i-th step are obtained by the least square fit to four strains $\varepsilon_k^{(i)} = 1$ to 4. Then, $N_s^{(i)}$, $N_c^{(i)}$, $M_s^{(i)}$, and $M^{(i)}$ are obtained as follows:

$$N_s^{(i)} = \varepsilon_s^{(i)} E A_s, \quad N_c^{(i)} = -N_s^{(i)}$$

$$M_s^{(i)} = \varphi_s^{(i)} E I_s, \quad M^{(i)} = M_s^{(i)} + N_s^{(i)} y_c \qquad \text{(1a-d)}$$

where E = steel Young's modulus, A_s and I_s = steel beam portion cross section and moment of inertia, respectively, y_c = distance between the centroids of the steel beam and concrete slab. This method does not require the value of concrete slab strain, slab effective width, or slip between the slab and steel beam.

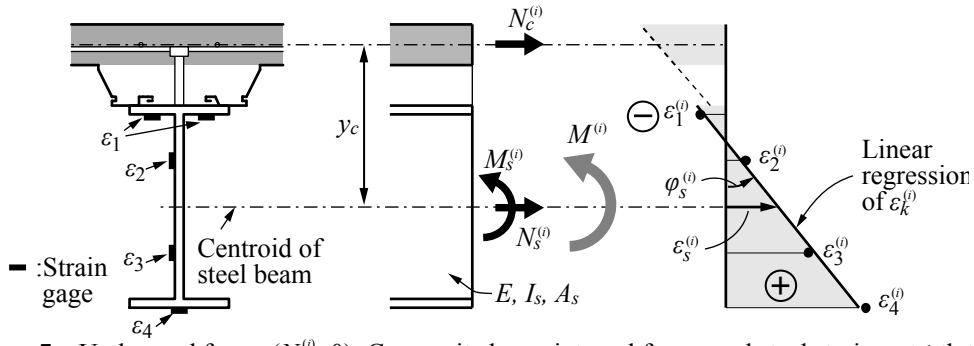

Figure 7 Undamped frame ($N^{(i)}$=0): Composite beam internal forces and steel strains, at i-th time step

As for the damped frame in Figure 6b, the beam axial force $N^{(i)} \neq 0$ results in change of the neutral axis location $e'^{(i)}$ as shown in Figure 8a, and the values of $N_s^{(i)}$, $N_c^{(i)}$, $N^{(i)}$, $M_s^{(i)}$, $M^{(i)}$ and $e'^{(i)}$ must be found. For this purpose, frame and damper action components $\varepsilon_{Fk}^{(i)}$ and $\varepsilon_{Dk}^{(i)}$ will be extracted from the recorded k-th strain $\varepsilon_k^{(i)}$ at the i-th step (Figure 8a). The phases of the frame and damper actions are assumed to be represented by bending moment of the closest column $M_{col}^{(i)}$ and axial force of the damper below the beam $F_{damp}^{(i)}$, respectively. The composite beam is assumed to be elastic but have higher and lower stiffness under positive and negative bending, respectively. Thus, by extrapolating $\varepsilon_k^{(i)}$-values and estimating the strain at the slab centroid, the strain data is grouped into two sets showing positive and negative strains. For each set, multipliers λ_{Fk} and λ_{Dk} to minimize the following R_k are obtained.

$$R_k = \sum_i \left\{ \varepsilon_k^{(i)} - \left(\varepsilon_{Fk}^{(i)} + \varepsilon_{Dk}^{(i)} \right) \right\}^2, \quad \varepsilon_{Fk}^{(i)} = \lambda_{Fk} M_{col}^{(i)}, \quad \varepsilon_{Dk}^{(i)} = \lambda_{Dk} F_{damp}^{(i)} \qquad \text{(2a-c)}$$

It is noteworthy that each $\varepsilon_k^{(i)}$ and thus-found $\varepsilon_{Fk}^{(i)}$ and $\varepsilon_{Dk}^{(i)}$ appear to be almost linearly distributed even under the combined frame and damper actions. Therefore, assuming plane section for each action at every i-th step, the curvature $\varphi_F^{(i)}$, $\varphi_D^{(i)}$ and the average axial strain $\varepsilon_a^{(i)}$ and $\varepsilon_b^{(i)}$ are obtained by the least square fit to strains $\varepsilon_1^{(i)}$ to $\varepsilon_4^{(i)}$ (Figure 7). Using them, all the above-listed values are obtained from the following equations:

$$N_s^{(i)} = (\varepsilon_a^{(i)} + \varepsilon_b^{(i)}) EA \quad , \quad N_c^{(i)} = \left\{ \varepsilon_a^{(i)} e'^{(i)} / (y_c - e'^{(i)}) - \varepsilon_b^{(i)} \right\} EA_s \quad , \quad N^{(i)} = N_s^{(i)} + N_c^{(i)}$$

$$M_s^{(i)} = (\varphi_F^{(i)} + \varphi_D^{(i)}) EI_s \quad , \quad M^{(i)} = M_s^{(i)} + N_s^{(i)} y_c - N^{(i)} (y_c - e'^{(i)}) \qquad \text{(3a-e)}$$

where, $e'^{(i)}$ is obtained from Figure 8a, and is assumed to be common for both frame and damper force actions. The moment obtained by this method was reasonably accurate, satisfying the joint equilibrium with the steel columns whose moments were directly estimated.

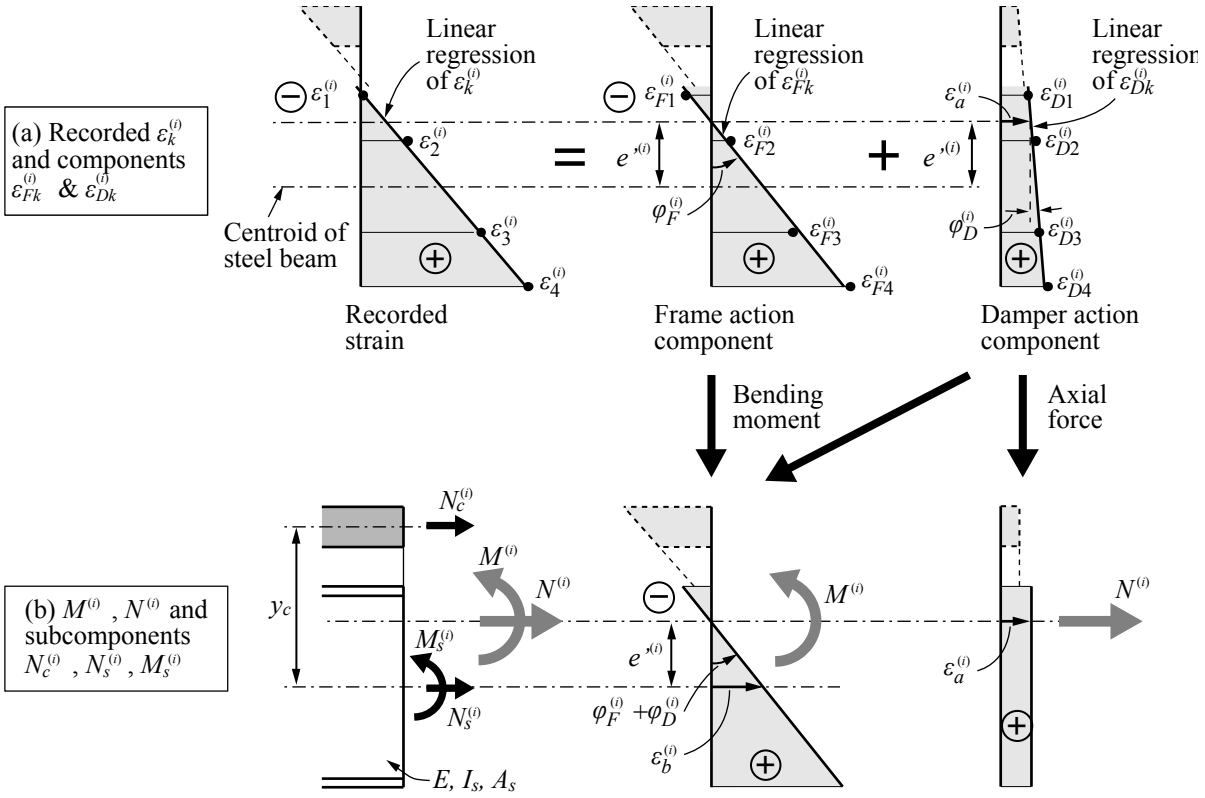

Figure 8 Damped frame ($N^{(i)}\neq 0$): Composite beam internal forces and steel strains, at *i*-th time step

2.3 Strain Decomposition: Validations and Findings

The above section has proposed the method to obtain frame and damper action components $\varepsilon_{Fk}^{(i)}$ and $\varepsilon_{Dk}^{(i)}$ from the recorded strain $\varepsilon_k^{(i)}$. In this chapter, the experimental data obtained from the 5-story building with steel damper using the Takatori ground motion (Section 2.1) is considered. As the first step of validating the method, choice of $M_{col}^{(i)}$ to represent the frame action component is examined. Figure 9 shows the case of undamped frame having only the frame action component, and the strain $\varepsilon_4^{(i)}$ is compared with $M_{col}^{(i)}$. Three cases (Figure 5) of the beam without slab, with slab extending to one side (one side slab), and with slab extending to two sides (two sides slab) located at the 4th floor are shown. They are very closely related, and demonstrate reasonableness of choosing $M_{col}^{(i)}$ to represent the frame action.

Figure 10 shows the case of damped frame having both the frame action and damper action components, and the recorded strain $\varepsilon_4^{(i)}$ is decomposed into $\varepsilon_{F4}^{(i)}$ and $\varepsilon_{D4}^{(i)}$. Like the above discussion, three cases of the slab attachment at the 4th floor are shown. Regardless of the extent of slab contribution, sum of the $\varepsilon_{F4}^{(i)}$ and $\varepsilon_{D4}^{(i)}$ closely agrees with $\varepsilon_4^{(i)}$, indicating accuracy of using linear combinations $\varepsilon_{F4}^{(i)} + \varepsilon_{D4}^{(i)}$ to represent $\varepsilon_4^{(i)}$. Note that the accuracy was confirmed also for strains $\varepsilon_1^{(i)}$ to $\varepsilon_3^{(i)}$, where $\varepsilon_{F4}^{(i)}$ was large at the bottom flange and $\varepsilon_{D4}^{(i)}$ was large near the neutral axis, respectively.

Figures 11 shows $\varepsilon_k^{(i)}$ recorded at the positive and negative peak moments in the undamped frame ($N^{(i)} = 0$), where three cases of the slab attachment at the 4th floor are shown. The strains are almost linearly distributed, justifying the assumption of plane section. When no slab is attached, neutral axis is at the mid-height of the steel beam section (Figure 11 left), since $N^{(i)} = 0$. It is considerably higher when the slab is attached, and becomes as high as the top flange of the steel beam (Figure 11 right). Note also that the negative bending case still shows significant composite action, as depicted by high locations of the neutral axis. This is contrary to the typical consideration, but similar results have been obtained from full-scale frame tests elsewhere (Kasai et al., 2005).

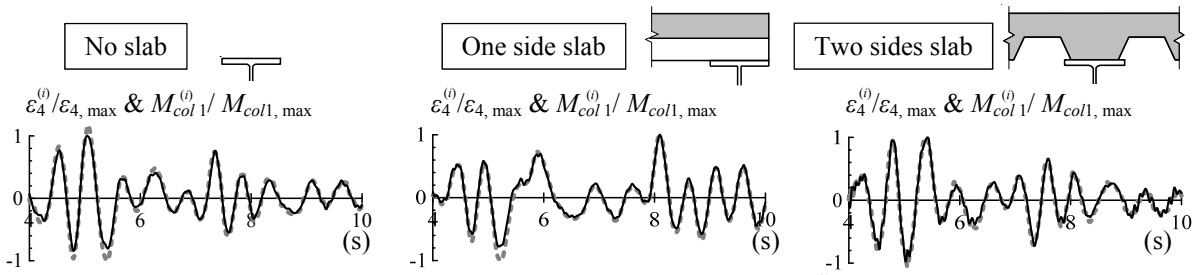

Figure 9 Undamped frame: Normalized steel strain at the bottom flange $\varepsilon_4^{(i)}/\varepsilon_{4,\max}$ and column moment $M_{col1}^{(i)}/M_{col1,\max}$ in three cases of slab attachment (— $\varepsilon_4^{(i)}/\varepsilon_{4,\max}$ - - - $M_{col\,1}^{(i)}/M_{col1,\max}$)

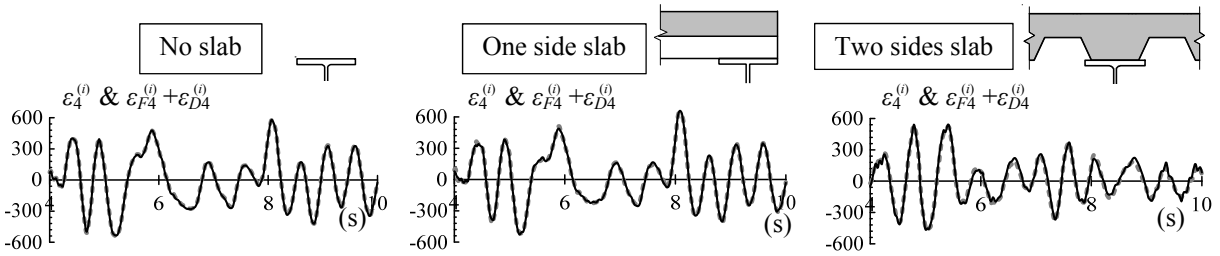

Figure 10 Damped frame: Steel beam strains (unit: micro-strain) at bottom flange in three cases of slab attachment, recorded steel strain $\varepsilon_4^{(i)}$ vs. combined frame and damper action components $\varepsilon_{F4}^{(i)}+\varepsilon_{D4}^{(i)}$
(— $\varepsilon_4^{(i)}$ - - - $\varepsilon_{F4}^{(i)}+\varepsilon_{D4}^{(i)}$)

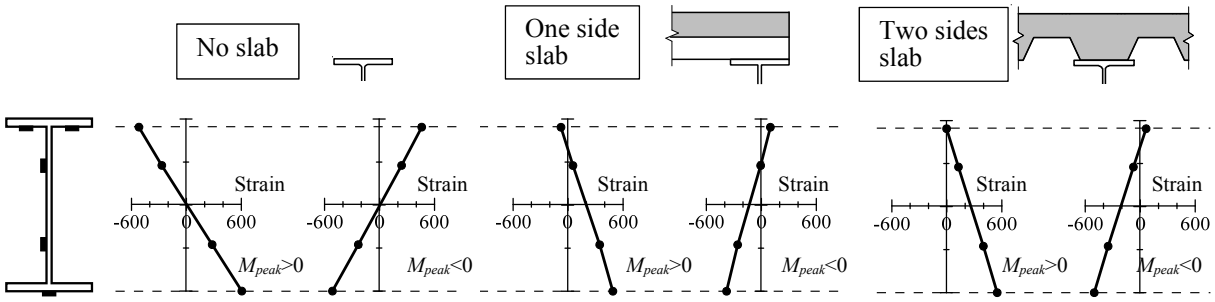

Figure 11 Undamped frame: Strain distributions $\varepsilon_k^{(i)}$, k=1 to 4, see Fig.7 (unit: micro-strain)

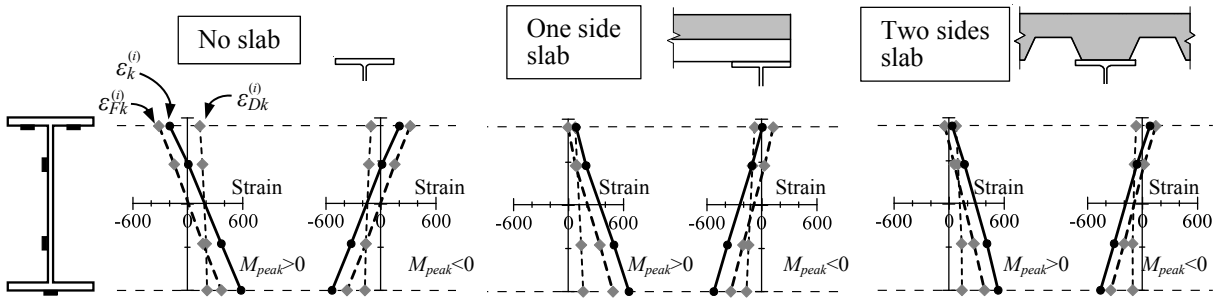

Figure 12 Damped frame: Strain distributions $\varepsilon_k^{(i)}$ vs. frame and damper action components $\varepsilon_{Fk}^{(i)}$, $\varepsilon_{Dk}^{(i)}$, k=1 to 4, see Fig.8 (unit: micro-strain)

In Figure 12, the black dots and solid lines show the $\varepsilon_k^{(i)}$ recorded at the positive and negative peak moments in the damped frame ($N^{(i)} \neq 0$). Almost linearly distributed strains, like those in the undamped frame above, justify the assumption of plane section for the present decomposition method. In the bare steel beam, the neutral axis shifts upward for both positive and negative moments (Figure 12 left), since $N^{(i)}$ produces axial strains $\varepsilon_{Dk}^{(i)}$ in the opposite direction of $\varepsilon_{Fk}^{(i)}$ at the upper cross section. Because of this, the neutral axis in the composite beam (Figure 12 middle & right) tends even higher than in the undamped frame.

In addition to the recorded $\varepsilon_k^{(i)}$, the frame and damper action components $\varepsilon_{Fk}^{(i)}$ and $\varepsilon_{Dk}^{(i)}$ are shown by the broken lines in Figure 12. The value of $\varepsilon_{Fk}^{(i)} + \varepsilon_{Dk}^{(i)}$ is about equal to the value $\varepsilon_k^{(i)}$, indicating accuracy of the decomposition. Linearly distributed $\varepsilon_{Fk}^{(i)}$ and $\varepsilon_{Dk}^{(i)}$ also justify the assumption of plane section for both frame and damper actions, and they show almost the patterns of bending and axial loads. Note that $\varepsilon_{Fk}^{(i)}$ at negative bending

case indicates very low neutral axis location $e'^{(i)}$, suggesting reduction of flexural stiffness. This is because slab is under tension due to negative bending, overcoming the effect of compressive axial force in the beam.

2.4 Internal Force Estimations: Validations and Findings

Using the 3D response data of the 5-story building, member and joint forces are obtained for all of 60 beams (6 frames x 10 beams), 90 columns (6 frames x 10 columns), and 90 joints (6 frames x 9 joints). $M^{(i)}$ and $N^{(i)}$ at a section of beam (Section 2.2.) are obtained by using Equations 1 (undamped frames) or 3 (damped frame), respectively. The column member forces are obtained directly from the strains at the two different vertical locations. Four gages are attached to the sides of the square tube column. For every beam and column, the moments at two sections are extrapolated to obtain the joint moment.

In order to examine accuracy of $M^{(i)}$ and $N^{(i)}$ at every *i*-th step, Figure 13a compares the sum of beam moments with the sum of column moments at the joint between two undamped frames, and Figure 13b compares those between undamped and damped frames. Figure 13c compares the axial forces obtained at the two sections of the composite beam (Section 2.2.). Estimated moments satisfy the joint equilibrium very accurately in the undamped frames ($N^{(i)} = 0$, Figure 13a). Between the undamped frame and damped frame ($N^{(i)} \neq 0$, Figure 13b), the accuracy is less but is reasonable especially at the peak responses. Figure 13c indicates some scatter of axial force $N^{(i)}$ at two sections in distance of 0.3 to 0.5 times the span length, where axial force is not expected vary significantly. It is felt that that even the strains corresponding to peak axial force are relatively small (Figure 12), and the error may be inevitable for smaller strains. However, the less scatter is observed for the peak responses. Figure 14 shows examples for moment diagram of the frames in X- and Y-directions (Figure 5), respectively, at the time of the largest base shear. As recognized from Figures 14, joint equilibrium is approximately satisfied in the 30 joints shown, confirming reasonable accuracy of the method proposed in Section 2.3.

The $M^{(i)}$ and $M_s^{(i)}$ are plotted in Figure 15a for the undamped frame ($N^{(i)}$=0) and in Figure 15b for the damped

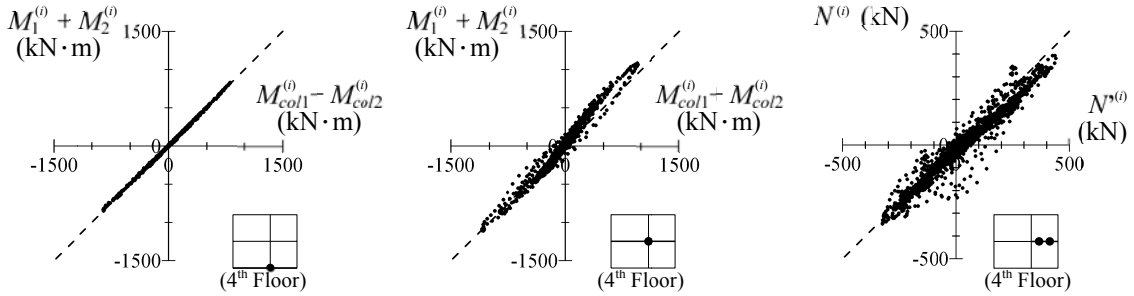

(a) Undamped frame: Moment equilibrium

(b) Damped frame: Moment equilibrium

(c) Damped frame: Axial equilibrium

Figure 13 Joint equilibrium of beam and column

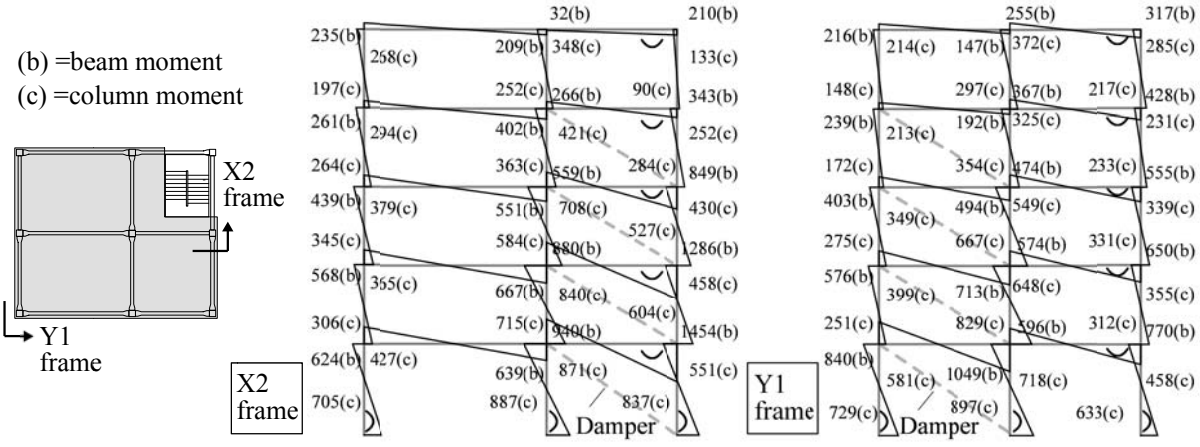

Figure 14 Moment distributions at the time of largest base shear (unit: kN·m)

frame ($N^{(i)} \neq 0$), in order to understand the contributions of the steel beam portion in the composite beam. $M_s^{(i)}$ appears to be half or less compared with $M^{(i)}$ for both positive and negative bending cases, indicating significant composite effect even for the latter. Similarly, $N^{(i)}$ and $N_s^{(i)}$ are also plotted in Figure 16. Even in the undamped frame where $N^{(i)} = 0$ (Figure 16a), significant $N_s^{(i)}$ develops due to the composite action regardless of the positive and negative loading cases. In the damped frame, $N_s^{(i)}$ appears to be even larger (Figure 16b) due to the damper force transmitted. The steel beam portion, therefore, appears to develop local axial force $N_s^{(i)}$ considerably larger than total axial force $N^{(i)}$ of the composite beam. Although $M_s^{(i)}$ is reduced, this indicate possibility of larger strain in the bottom flange of the steel beam portion.

From the moment diagram of Figure 14 shown earlier, the positive moment is about 1.2 time the negative moment in the undamped frame, whereas it becomes larger in the damped frames. It is about 1.5 times in the damped frame of the X2 frame, where the damper is twice larger than the other two (Section 2.1). This lead to larger tension forces in the composite beam while the concrete is still in compression, and effectively increased the moment arm of the stress block (Figures 12 and 15: two sides slab). However, this also means smaller moment under negative bending, due to tension and eventually cracking of the concrete as discussed (Section 2.3). Note also that these situations can change, depending on relative sizes of steel beam, slab, and damper.

The above-mentioned relationships among beam axial force, positive and negative moments, and their effects on beam stiffness seem complex and requires further study. This paper only provide introductory remarks: The concrete slab is assumed to share the plane section with the steel beam by considering no slips between them. Then, from the recorded steel strains, concrete strain $\varepsilon_c^{(i)}$ is obtained by extrapolation. Since $N_c^{(i)}$ is estimated from Eq. 3b and E_c is given, slab effective width $B = N_c^{(i)} / (E_c \varepsilon_c^{(i)} t)$, where t = slab thickness. Finally, the composite

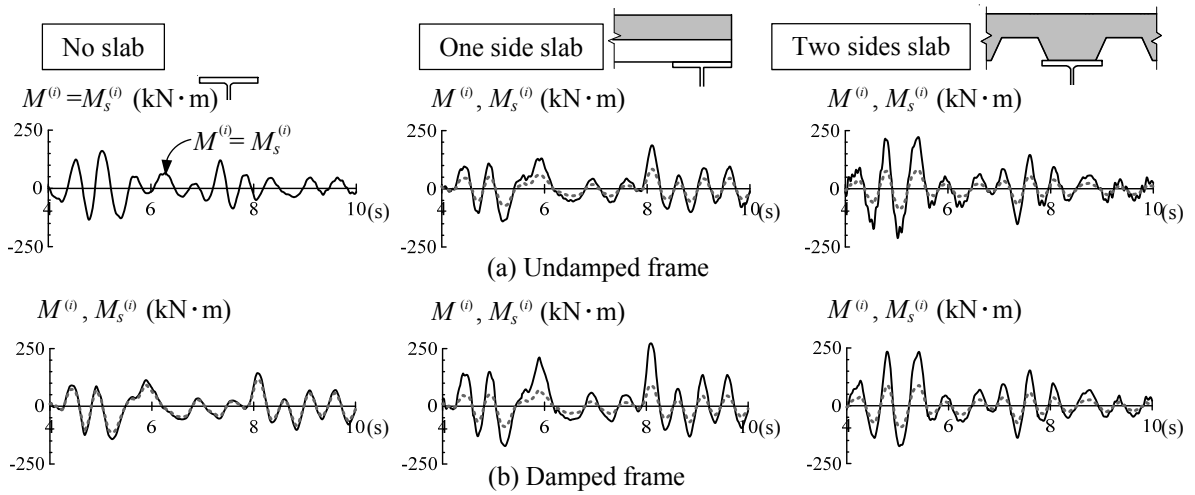

Figure 15 Composite beam moment $M^{(i)}$ vs. steel beam moment $M_s^{(i)}$ (— $M^{(i)}$ ····· $M_s^{(i)}$)

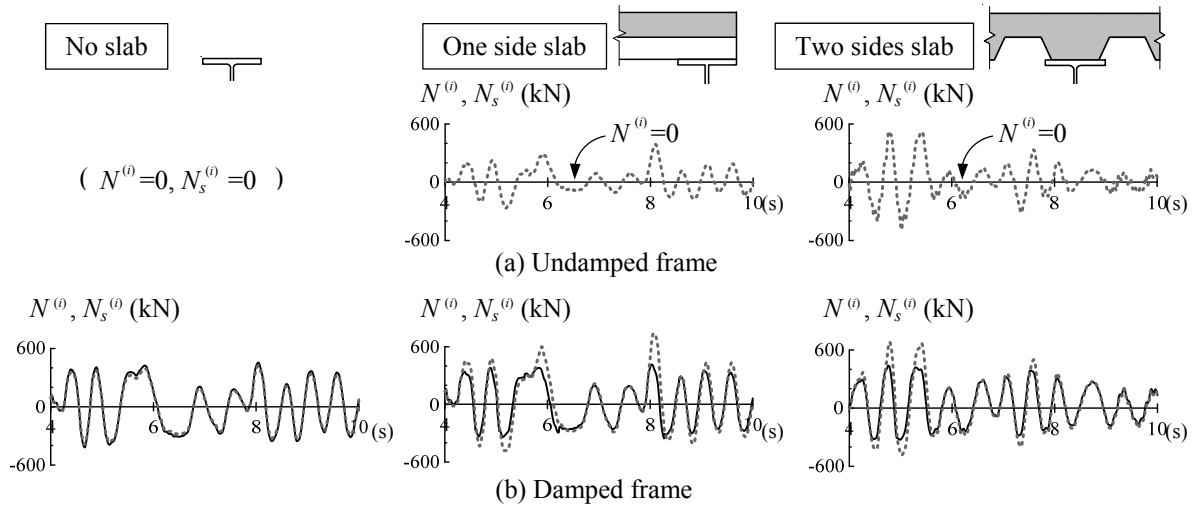

Figure 16 Composite beam axial force $N^{(i)}$ vs. steel beam axial force $N_s^{(i)}$ (— $N^{(i)}$ ····· $N_s^{(i)}$)

moment of inertia I can be calculated. In Figure 17, average of I/I_s values at the two sections under positive bending are indicated for every beam on the 4th floor. The beams in Figures 11 and 12 (two sides slab) subjected to the Takatori ground motion are used. The values are very large, varying from 2.38 to 3.0. Figure 18a indicates thus-calculated B, corresponding $e'^{(i)}$, and I/I_s for the undamped frame ($N^{(i)} = 0$). The values are only 10 % different between the positive and negative loading cases. Whereas in Figure 18b ($N^{(i)} \neq 0$), they are less than half the values of positive loading case, as discussed earlier. Except for this case, B is 0.7 to 0.8 times the effective width of 1,200 mm estimated from the Japanese specification (AIJ, 2010).

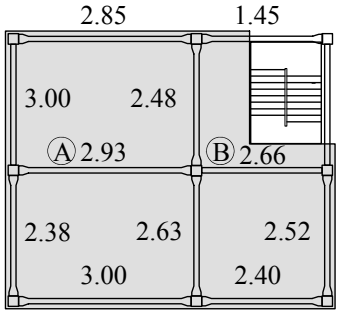

Figure 17 Distribution of I/I_s at positive bending

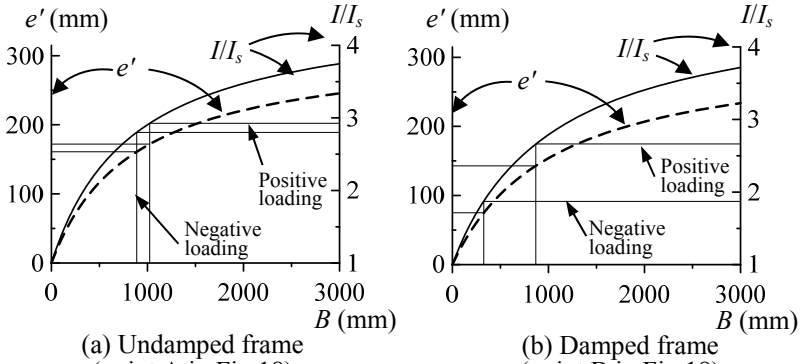

(a) Undamped frame (point A in Fig.18)

(b) Damped frame (point B in Fig.18)

Figure 18 Conversion from neutral axis location e' to composite stiffness ratio I/I_s and slab effective width B

3. FULL-SCALE SUBASSEMBLY SUBJECTED TO FRAME & DAMPER ACTIONS

The full-scale building shake table test discussed above is probably the most realistic simulation method for seismic behavior. By numerous sensors and proposed data analysis method, internal forces of all members including dampers have been found, and they would be very useful in clarifying the effects of frame and damper actions on local and global responses of the building.

On the other hand, such extensive instrumentations are still not dense enough to find more details of local behavior for the members and connections. The full-scale subassembly test to supplement such information, therefore, is important experimental method. Unlike the full-scale building test limited to one or only a few specimens, a large number of subassemblies could be tested systematically by varying pertinent parameters. In order to fully realize such advantages, the test set-up must be compact and convenient for mantling/dismantling the specimen, and loading method and boundary conditions must, although not truly realistic, reflect important features. This chapter discusses the test with such loading method as well as another applications of the data analysis method presented in Chapter 2, all of which consider the frame and damper actions.

3.1 Hybrid Test Combining Frame and Damper Actions

Figure 19a shows the concept of a simplified hybrid test method combining actions of a subassembly and a virtual damper. The subassembly has a configuration of L-shape, representing a quarter portion of the frame. In order to be consistent with Chapter 2, "positive loading" is defined to cause axial tension and positive moment for the beam, and vice versa (Figure 19b). Figure 20 shows the test set-up, where laterally supported L-shape specimen is connected to two links that keep the distance between the midpoint of the brace and inflection points in beam and column, respectively.

Two parallel actuators (total 3,000 kN capacity) are used for the displacement control to satisfy the target story drift u or story drift angle $\theta = u/H$, and one oil jack diagonally placed (1,400 kN capacity) for the force control simulating damper force F_{damp}. The target u reflects the frame action, and the target F_{damp} reflects damper action. The target F_{damp} depends on the change Δu_a in diagonal distance (Figure 20) due to local deformations such as gusset plate yielding, axial contraction of the beam due to local buckling, and so on. Target F_{damp} is calculated by substituting the measured Δu_a into the mathematical model of the damper (virtual damper) at every step of the test. The virtual damper can be of any damper type, as long as the mathematical model is available. The steps for displacement control, force control, and damper force calculation are shown in Figure 20.

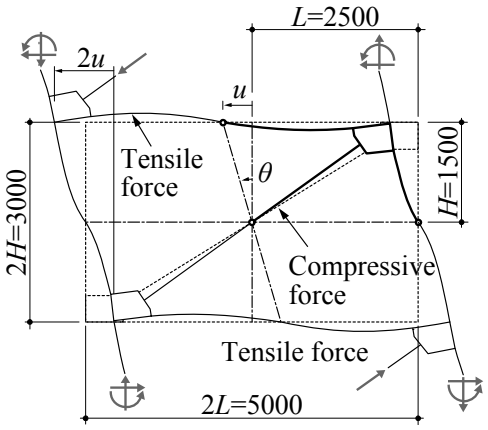

Figure 19a Assumed displacement field for simplified hybrid test method

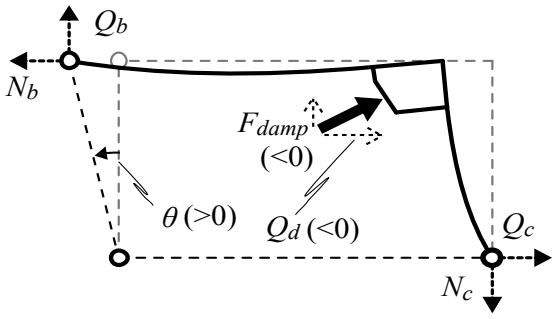

Figure 19b Definition of positive loading case

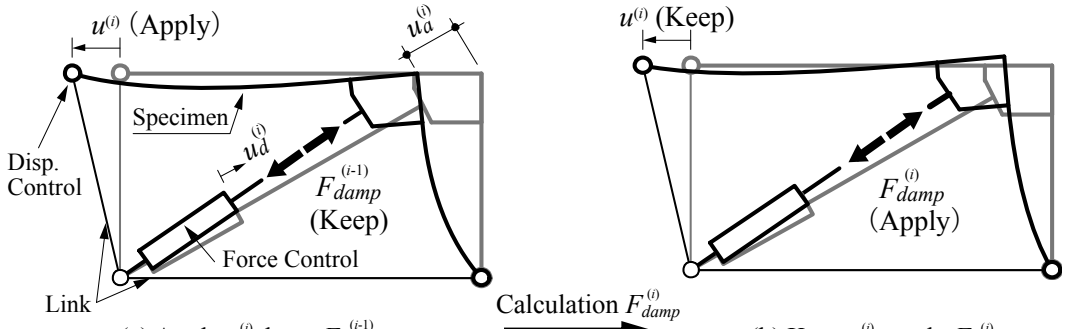

(a) Apply $u^{(i)}$, keep $F_{damp}^{(i-1)}$ (b) Keep $u^{(i)}$, apply $F_{damp}^{(i)}$

Figure 20 Loading method in *i*-th step

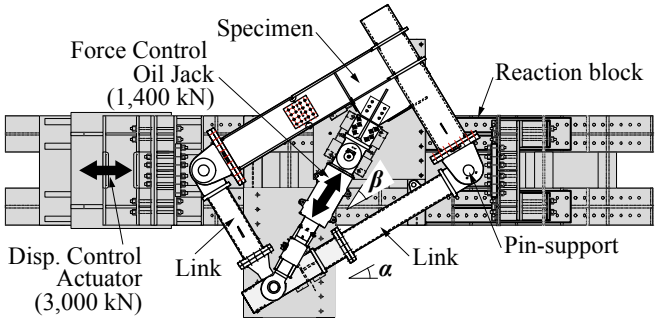

Figure 21a Set-up of full-scale subassembly test

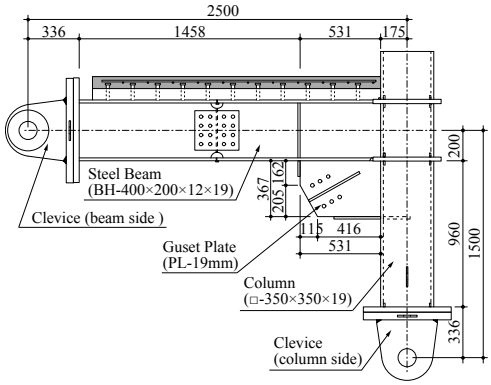

Figure 21b Subassembly specimen

Figure 21 shows the set-up and the specimen. The specimen geometry and material are identical with those in the full-scale frame explained in Chapter 2. The beams are the same as described in Section 2.1, and the typical specimen is a built-up section of BH-400×200×12×19 (400 mm deep, 12 mm thick web, 200 mm wide and 19 mm thick flange). The column is a square box section of □-350×350×19. The nominal yield strength of the steel material is 325 MPa for all the elements, and actual yield stresses are 365, 390, 398, and 401 MPa for the beam web, flange, column, and gusset plate, respectively. 8 specimens of this size with varied details were tested, and 17 specimens of larger size (BH-500×250×12×22, □-400×400×19) had been tested (e.g., Kasai et al. 2015)

Figure 22 shows the test results using the larger specimens mentioned above. The virtual dampers were the steel damper, viscoelastic damper, and friction damper, respe ctively. The damper force horizontal component Q_d, frame horizontal force Q_f, and system horizontal force Q_s are shown. The target Q_d and applied Q_d are shown in the same graph by the gray and black solid lines, respectively. As understood from Figures 22a and b, the force control of the virtual steel and viscoelastic dampers was reasonably accurate. Note that for the friction damper, calculated target force F_{damp} was too sensitive to Δu_a (Figure 20) during unloading, because of its large elastic stiffness. Thus, instead of calculating the target F_{damp}, the sign of the slip force $\pm F_{dy}$ is reversed and used as the target F_{damp}. This resulted in rigid-plastic damper performance, causing abrupt changes in strains in the

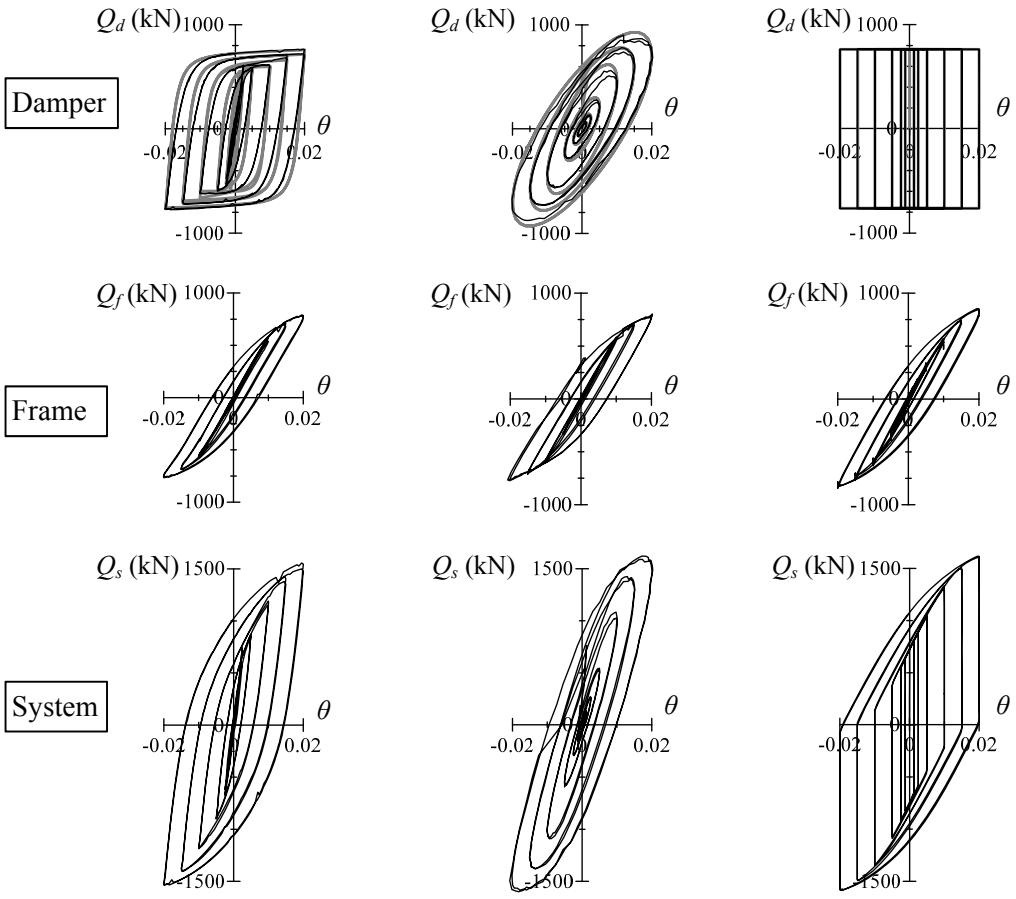

(a) With steel damper (b) With viscoelastic damper (c) With friction damper

Figure 22 Test results for damper, frame, and system action (three types of dampers, bare steel baem)
(—— Recorded —— Target (only Q_d))

subassembly. Such behavior is considered to show an extreme and interesting case of the elasto-plastic damper, and was investigated further.

The frame action can be observed from the Q_f–curves in Figure 22. The first yielding occurred at about θ = ±0.5% rad, due the stress concentration at the bottom flange immediately outside the gusset plate connection. Significant reduction in horizontal stiffness occurs due to further beam yielding at θ= ±1% rad. As will be shown, the beam fully yields at θ= ±1.5% and remain stable up to θ= ±2% rad and larger except for some specimens (Kasai et al. 2015). Figure 23 shows the interaction of beam axial force N and bending moment M normalized by the yield axial force N_y and full plastic moment M_p, respectively.

Because of the L-shape, the M - N relationship becomes analogous to Q_s – θ relationship. The fatness of these loops indicate extent of the phase difference between the force and deformation and corresponding equivalent damping of the system. The system using the friction damper with idealized rigid unloading stiffness gives the largest energy dissipation and damping. Figure 23 shows that beams of all three systems reach full plastic state at a story drift angle θ= ±1.5% and N / N_y ≈ 0.25. Among the three systems, yielding of the beam was most

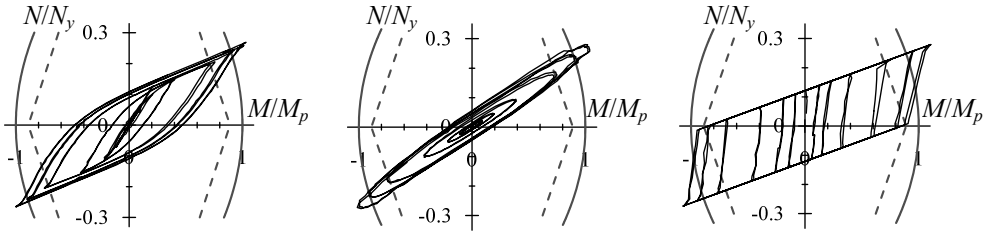

(a) With steel damper (b) With viscoelastic damper (c) With friction damper

Figure 23 Interaction between beam moment M/M_p and N/N_y (bare steel beam)

significant in the system with friction damper, as suggested by the large beam moment even after unloading in Figure 23.

3.2 Beam Strain Decomposition: Validations and Findings

Figure 24 shows the composite beam specimen with the size smaller than discussed above. The specimen geometry and material are identical with those in the full-scale frame explained in Section 2.1, and is BH-400×200×12×19. The column is a square box section of □-350×350×19. The specimen was subjected to cyclic load test, result of which is processed by the data analysis method proposed in Chapter 2. Equation 2 is applied up to the end of the second cycle of the peak story drift angle $\theta=\pm 1/200$. Unlike the frame test in Chapter 2, the beam moment $M^{(i)}$ and axial load $N^{(i)}$ are directly measured, and accuracy of their estimations made by the data analysis method is directly assessed.

From the data of such a test, the responses at θ= 1/200 rad and F_{damp} = -675kN, and θ = -1/200 rad and F_{damp} = +705kN are selected to extract the frame and damper action components. In Figure 24, the frame and damper action components (broken lines) are obtained by the method proposed in Chapter 2. At Section C1 whose distance from the face of the vertical stiffener for the gusset plate is 0.4 times the beam depth, the plane section remains approximately plane in both frame (Figure 24a) and damper (Figure 24b) action components. But at Section C2, whose distance is only 0.09 times the beam depth, stress at the bottom flange is concentrated and is about 2 times the value extrapolated from the strains in the upper half of the section for both positive and negative loading cases. In the positive bending case where beam axial force is tension, the neutral axis is much higher than the negative loading case, which is in conformity with the findings from the full-scale building test (Section 2.3).

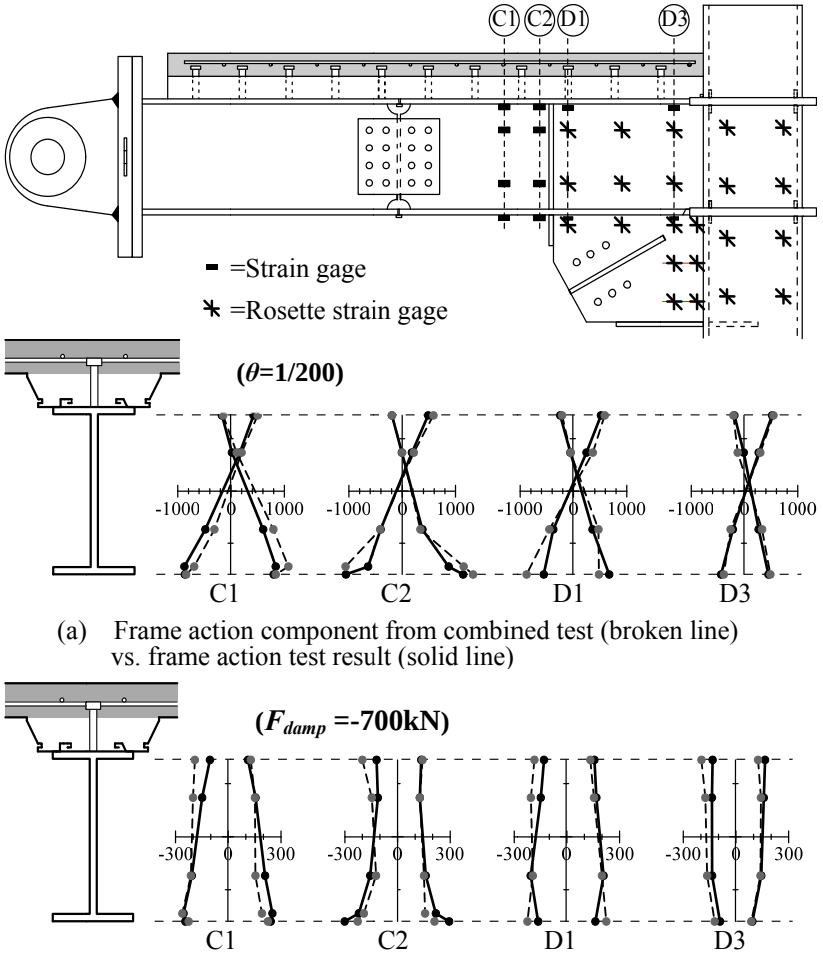

Figure 24 Composite beam strain distributions in subassembly test

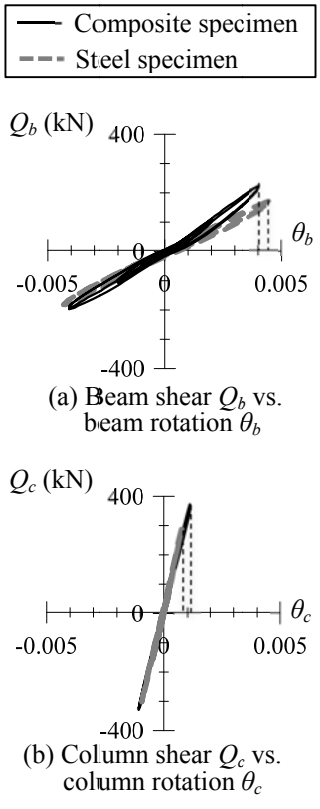

Figure 25 Frame action test (θ=1/200): (a) Q_b vs. θ_b, and (b) Q_c vs. θ_c

In this section, separate tests, namely, “frame action test” applying θ= ±1/200 rad and F_{damp} = 0, and “damper action test” applying F_{damp} = ±700kN and θ=0 are conducted. The separate test results are shown by the solid lines, and appear to agree well with the values of frame and damper action components obtained above (broken lines). In these tests reflecting the frame action and damper action separately, the strains as well as $N_s^{(i)}$, $N_c^{(i)}$, $M_s^{(i)}$, and $e'^{(i)}$ (Section 2.2) are also compared with frame and damper action components obtained from the combined test using the data analysis method. In this manner, accuracy of the data analysis method proposed in Chapter 2 for the beam strains as well as internal forces has been validated.

Figure 25a also shows the result of the frame action test. It plots beam shear vs. beam chord rotation relative to the cross-sectional plane defined at 275 mm (half of the gusset plate length) from the column face. The bare steel subassembly test result is also plotted, and the composite beam chord rotation is 0.9 times and 0.95 times, shear force is 1.28 times, and 1.08 times those of the steel subassembly, respectively. Because of this the column shear force and chord rotation increase and becomes larger than the steel subassembly, especially at positive loading (Figure 25b).

3.3 Gusset Plate Strain Decomposition: Validations and Findings

In this section, data analysis will be extended to highly non-uniform strains in the gusset plate connections. Equation 2 is applied to the strain gages in Figure 26, where the total number *k* of the strain gages in the rosette and others is 66. Like Section 3.2, Equation 2 is applied up to the end of the second cycle of the peak story drift angle θ=±1/200. After obtaining the frame and damper action components, principal strains and directions are calculated and plotted. Figure 26 shows such a result at θ=+1/200, F_{damp} =-700kN, and sum of the two components. Direction of principal strains of frame action component is about same as that of damper action component (Figure26a, b), except for panel area in which they are opposite.

Thus, in both positive and negative loading cases, the strains in the connection will increase by combining the two actions, whereas those in the panel decrease. In the gusset plate, the frame action component shows largest principal strains near the beam flange (790 micro-strain) and near the column face (690 micro-strain) at θ=+1/200. On the other hand, the damper action component shows only small principal strains. Thus, the gusset plate has much reserved strength against the damper action. It is governed by the frame action and would yield at θ=±1/100, which however could be avoided by simply increasing the plate thickness. The Japanese criteria of gusset plate considers only damper force, but it should consider the frame action discussed here.

As the separate tests, the results from the frame action test and damper action test are shown in Figures 27a and b, respectively. They are analogous to plots of the frame and damper action components extracted from the combined test by using the proposed data analysis method. Using the method, therefore, participations of the frame and damper actions will be clarified without conducting separate test, and could effectively predict the hypothetical case of different balance of the two actions. Moreover, using the plots shown in Figure 28, the time history curve of the damper action may be shifted or its shape may be modified (e.g., to sine wave for viscoelastic case) to examine the effects on the superposed responses.

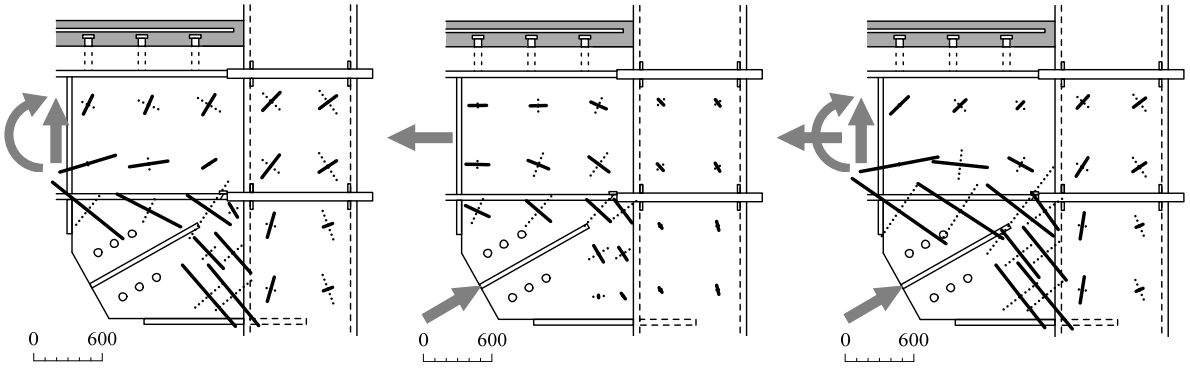

(a) Frame action component at θ=+1/200 (b) Damper action component at F_{damp} =-700kN (c) Sum of the two components at θ=+1/200 and F_{damp} =-700kN

Figure 26 Combined test: Decomposition of principal strains recorded at θ=+1/200, F_{damp} =-700kN, and sum of the two components (unit: micro-strain)

Solid line=tensile strain
Broken line=compression strain

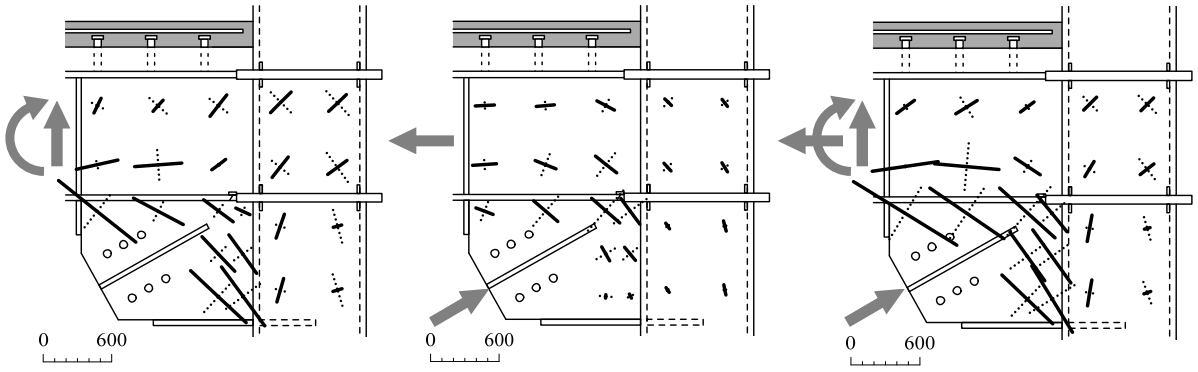

(a) Frame action test at θ=+1/200 (b) Damper action test at F_{damp} =-700kN (c) Superposition

Figure 27 Separate tests: Recorded principal strains at three different tests (unit: micro-strain)

Solid line=tensile strain
Broken line=compression strain

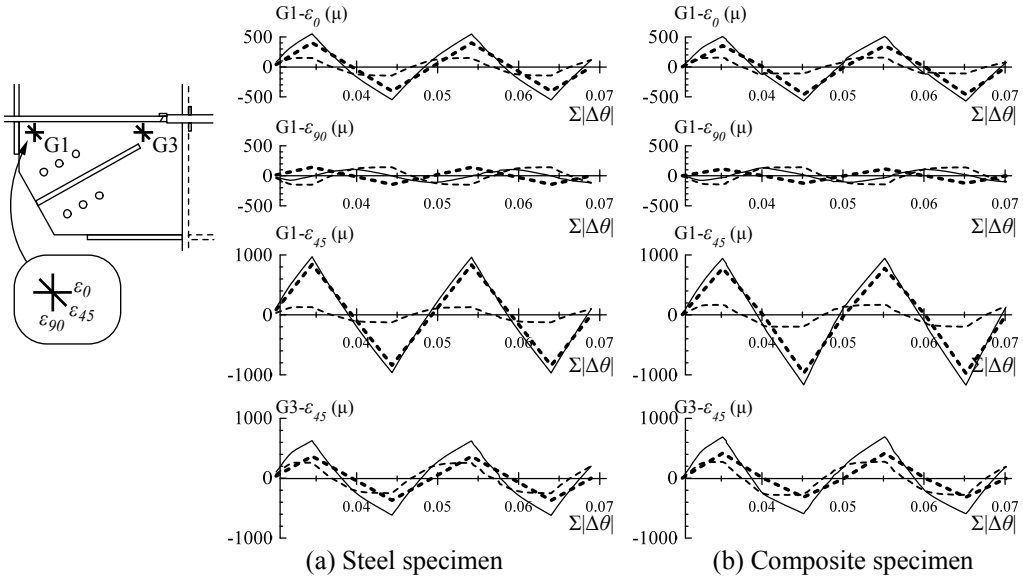

(a) Steel specimen (b) Composite specimen

Figure 28 Composite specimen: Decomposition of strains and their sum

(——— Combined ----- Frame action component -------- Damper action component)

4. CONCLUSIONS

In a supplementally-damped system, the composite beam is subjected to combinations of positive and negative bending produced by the frame action, and, especially where damper is attached, the compressive and tensile forces produced by the damper action. The composite beam behavior can significantly affect the overall frame stiffness as well as local strain distributions in the members and connections. This paper has investigated the issues based on full-scale experiments of 5-story building and subassemblies. The conclusions are as follows:

1. The composite action characterized by upward shifting of the beam neutral axis under positive bending and even negative bending was clearly observed from the strains recorded at the steel beam portions. Additional shifting occurs due to the beam axial force produced by the dampers.
2. Proposed data analysis method has decomposed the recorded strains into the frame action and damper action components based on phase difference between the two actions. Strains due to the frame and damper actions are linearly distributed and almost constant, each maintaining plane section.
3. Internal forces of the composite beam with and without axial forces are estimated for the two types of tests. They are verified through examinations of join equilibrium of the building, and direct comparison of the bending and axial loads measured from the subassembly.
4. Stiffness of the composite beam is estimated by using thus-found internal force and assuming plane section extended to the slab. It is somewhat smaller than the values from specifications, and is considerably smaller for negative bending and compressive axial load. Slip at slab-beam interface must be studied.
5. Proposed hybrid test method for the subassembly with simulated frame and damper actions performed well, producing realistic overall hysteresis and local behavior. Simultaneous displacement control and force control, connected by numerical simulation of the damper action, are performed.
6. Two-dimensional strains at the gusset plate of the subassembly are also decomposed, and highly non-uniform strains are clarified by combination of the two scaled actions. Contribution from each action is obtained without conducting separate test, and combined effects can be easily evaluated for design.

In addition to the experiment-based studies explained, analytical study of extended Newmark's composite beam theory as well as numerical simulations are being performed at Tokyo Institute of Technology.

REFERENCES

1. Kasai, K., Hikino, T., Ito, H., Ooki, Y., Kato, F., Baba, Y. (2011). Overall test outline and response of building without dampers, 3D shake table tests on full scale 5-story steel building with dampers Part1. *J. Struct. Constr. Eng.,* **No.663**, pp.997-1006.
2. Kasai, K., Baba, Y., Nishizawa, K., Hikino, T., Ito, H., Ooki, Y., Motoyui, S. (2012). Test results for building with steel dampers, 3D shake table tests on full scale 5-story steel building with dampers Part2. *J. Struct. Constr. Eng.,* **No.673**, pp. 499-508.
3. Kasai, K., Baba, Y., Ito, H., Tokoro, K., Hikino, T., Ooki, Y., Murai, R. (2012). 3-D shake table tests on full scale 5-story steel building with viscoelastic dampers. *J. Struct. Constr. Eng.,* **No.676**, pp. 985-994.
4. Kasai, K., Yamagiwa, H., Baba, Y., Ito, H., Hikino, T., Ooki, Y. (2013). 3-D shake table tests on full scale 5-story steel building with oil dampers. *J. Struct. Constr. Eng.,* **No.693**, pp. 1999-2008.
5. Kasai, K., Yamagiwa, H., Nishijima, M., Baba, Y., Ito, H., Hikino, T., Ooki, Y. (2014). 3-D shake table tests on full scale 5-story steel building with viscous dampers. *J. Struct. Constr. Eng.,* **No.695**, pp. 47-56.
6. Suita, K., Matsuoka, Y., Yamada, S., Shimada, Y., Tada, M., Kasai, K. (2009). Experimental procedure and elastic response characteristics of shaking table test, Complete collapse test of 4-story steel building Part 1. *J. Struct. Constr. Eng.,* **No.635**, pp. 157-166.
7. Yamada, S., Suita, K., Matsuoka, Y., Shimada, Y. (2009). Elasto-plastic responses and process leading to a collapse mechanism, Complete collapse test of 4-story steel building Part 2. *J. Struct. Constr. Eng.,* **No.644**, pp. 1851-1859.
8. Shimada, Y., Suita, K., Yamada, S., Matsuoka, Y., Tada, M., Ohsaki, M., Kasai, K. (2010). Collapse behavior on shaking table test, Complete collapse test of 4-story steel building Part 3. *J. Struct. Constr. Eng.,* **No.653**, pp. 1351-1360.
9. Matsumiya, T., Nakajima, M., Suita, K., Satoh, Y. (2005). Damage to beam and effects of floor slab composite action, Test on full-scale three story frame for evaluation of seismic performance. *J. Struct. Constr. Eng.,* **No.593**, pp. 177-184.

10. Matsumiya, T., Suita, K., Nakajima, M., Liu, D., Zhou, F., Mizobuchi, Y. (2005). Effect of RC floor slab on hysteretic characteristics of steel beams subjected to large cyclic loading, Test on full-scale steel frame with RC floor slab. *J. Struct. Constr. Eng.,* **No.598**, pp. 141-147.
11. Architecture Institute of Japan (2010). Design recommendations for composite constructions
12. Kasai, K., Matsuda, Y., Motoyui, S., Kishiki, S. (2005). Fundamental study using new test loading scheme for steel frame subassembly with damper connection details. *J. Struct. Constr. Eng.,* **No.708**, pp. 309-319.
13. Newmark, N.M., Siess, C.P., Viest, I.M. (1951). Test and analysis of composite beams with incomplete interaction, *Proceedings of the Society of Experimental Stress Analysis,* **9:1**, pp. 75-92.